

THz Letters

A 400-GHz Graphene FET Detector

Andrey A. Generalov, Michael A. Andersson, Xinxin Yang, Andrei Vorobiev, and Jan Stake

Abstract—This letter presents a graphene field effect transistor (GFET) detector at 400 GHz, with a maximum measured optical responsivity of 74 V/W, and a minimum noise-equivalent power of 130 pW/Hz^{1/2}. This letter shows how the detector performance degrades as a function of the residual carrier concentration in the graphene channel, which is an important material parameter that depends on the quality of the graphene sheet and contaminants introduced during the fabrication process. In this work, the exposure of the graphene channel to liquid processes is minimized resulting in a low residual carrier concentration. This is in part, an important contributing factor to achieve the record high GFET detector performance. Thus, our results show the importance to use graphene with high quality and the importance to minimize contamination during the fabrication process.

Index Terms—Detectors, field effect transistor (FET), graphene, submillimeter wave measurements, submillimeter wave transistors, terahertz (THz).

I. INTRODUCTION

DETECTORS based on field effect transistors (FETs) can be implemented in advanced IC technology. This offers high levels of integration and functionality, which are both required for future large sensor arrays and terahertz (THz) imaging systems. FET THz detectors have been realized in various technologies, including CMOS [1]–[4], AlGaIn/GaN [5], [6], InP [7], and graphene [8]–[10]. The implementation of graphene in FET THz detectors has the potential to achieve competitive sensitivity at room temperature operation. Furthermore, it allows us for the creation of fast and inexpensive THz detectors that are compatible with industrial CMOS processes. The best noise-equivalent power (NEP) achieved in graphene FET (GFET) detectors of 515 pW/Hz^{1/2} [8] indicates that they come close to competing with other types of room-temperature THz detectors [11].

In contrast with established MOSFET technology, GFETs have a strong performance variation depending on the methods of graphene transfer and fabrication of GFET devices [12]. In particular, during the lithographic wet processes, the contamination of the graphene surface results in reduction of the mobility of

Manuscript received January 17, 2017; revised March 16, 2017, May 5, 2017, and May 29, 2017; accepted June 26, 2017. This work was supported in part by Chalmers Area of Advance, in part by EU Graphene Flagship, and in part by the Knut and Alice Wallenberg Foundation. (Corresponding Author: Andrey A. Generalov.)

The authors are with the Terahertz and Millimetre Wave Laboratory, Department of Microtechnology and Nanoscience–MC2, Chalmers University of Technology, 41296 Göteborg, Sweden (e-mail: gandrej@chalmers.se).

Color versions of one or more of the figures in this letter are available online at <http://ieeexplore.ieee.org>.

Digital Object Identifier 10.1109/TTHZ.2017.2722360

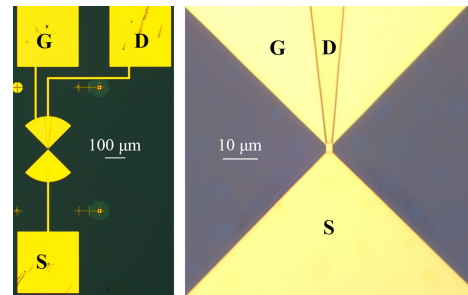


Fig. 1. Left: an optical microscope image of the fabricated GFET detector with contact pads (S, G, and D - source, gate, and drain, respectively). Right: a zoomed image of the GFET detector in the center of the bowtie antenna.

carriers [13] and also an increase of the residual carrier concentration n_0 [14], [15].

In this letter, we experimentally and theoretically demonstrate the dependences of maximum responsivity on n_0 in GFET THz detectors.

II. DESIGN

The bowtie antenna integrated with a GFET is shown in Fig. 1, which is a scaled design of the antenna reported in [8]. The gate dimensions of the GFET are a width $W_G = 2 \mu\text{m}$ and length $L_G = 2.5 \mu\text{m}$. The antenna radius is $160 \mu\text{m}$, which provides an almost constant impedance of 65Ω above 350 GHz. The antenna is placed in the center of a hyper-hemispherical lens, which is made of high-resistive silicon. It has a radius of 2.5 mm and a hyper-hemispherical extension of 0.75 mm.

The signal from the antenna is fed to the gate-source terminals. The gate-drain terminals have a capacitive coupling that is achieved by splitting the bowtie antenna, as shown in Fig. 1. Due to asymmetrical coupling, this FET detector has the capability of rectifying an RF signal into a dc response. The dc signal is measured at the source–drain terminals.

III. FABRICATION

The fabrication steps of the GFET detector are shown in Fig. 2. The high-resistivity Si substrate has a 300 nm SiO₂ layer that is covered with a single-layer CVD graphene using a dry transfer; this was supplied commercially by Graphenea, Inc., [16]. In the first step, the graphene layer was covered by a thin Al seed layer and followed by natural oxidation at 160 °C. An Al₂O₃ gate dielectric was then grown on top of the seed layer by atomic layer deposition [see Fig. 2(a)], resulting in a total oxide thickness of 18 nm. These steps prevent any liquids from coming into contact with the graphene in the FET channel during the next steps. This sets it apart from previously used technology

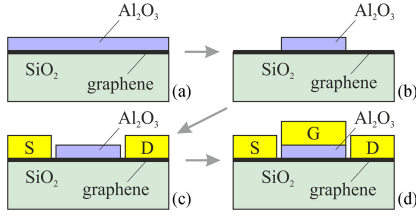


Fig. 2. Fabrication steps of the GFET detector.

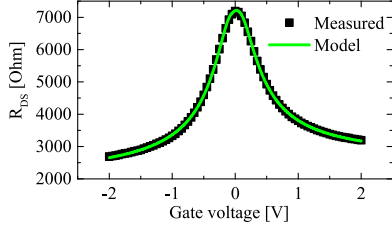


Fig. 3. Drain-source resistance of the GFET versus gate voltage.

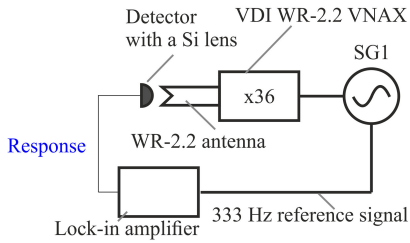


Fig. 4. Schematic image of the experimental setup.

[8] and also allows us for a cleaner gate dielectric/graphene interface with lower n_0 .

Next, the Al_2O_3 was patterned and etched with a buffered oxide etch [see Fig. 2(b)]. The source and drain contacts were fabricated by evaporating and patterning of 4 nm Ti, 10 nm Pd, and 290 nm Au [see Fig. 2(c)]. In the final step, the gate electrode was evaporated and patterned on top of the patterned Al_2O_3 layer with 10 nm Ti and 300 nm Au [see Fig. 2(d)]. An optical microscope image of the fabricated GFET detector is shown in Fig. 1. The chips are diced and mounted on a hyper-hemispherical silicon lens, and then bonded to a printed circuit board for contacting and measurements.

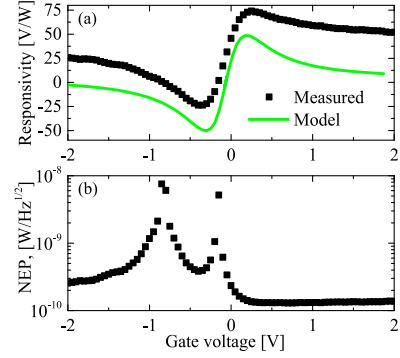
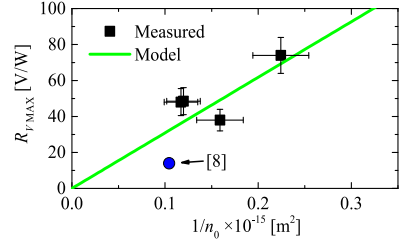
IV. RESULTS

A. DC-Characterization

The fabricated GFET detector was characterized under dc. The drain-source resistance versus the gate voltage is shown in Fig. 3, at a constant drain-source bias of 10 mV. The measured data is fitted by a semiempirical GFET model, as presented in [17]. The fitting parameters in the model are the residual carrier concentration n_0 , mobility of the electrons and holes μ_e and μ_h , and contact resistance. The values extracted from the fitting function in Fig. 3 are $\mu_h = 2800 \text{ cm}^2/\text{Vs}$, $\mu_e = 3100 \text{ cm}^2/\text{Vs}$, and $n_0 = 4.5 \cdot 10^{15} \text{ m}^{-2}$. The contact resistances are 2.0 and 2.5 $\text{k}\Omega$ for the hole and electron branches, respectively.

B. THz Detection

A schematic image of the experimental setup is shown in Fig. 4. A VDI WR-2.2 VNAX source was used at 400 GHz.

Fig. 5. (a) Measured voltage responsivity and (b) calculated from (2) NEP of the GFET detector with $n_0 = 4.5 \times 10^{15} \text{ m}^{-2}$ at 400 GHz.Fig. 6. Maximum responsivity of GFET detectors versus inverse residual carrier concentration $1/n_0$.

This was fed with the signal generator SG1, which provides amplitude modulation at a frequency of 333 Hz. The source irradiates the GFET detector through the WR-2.2 diagonal horn antenna. The response of the detector was measured with a lock-in amplifier. The voltage responsivity is calculated as follows:

$$R_V = 2\sqrt{2} \frac{V_{\text{lock-in}}}{P} \quad (1)$$

where P is the power measured at the input of the WR-2.2 horn antenna, with an Erickson calorimetric power meter. The factor $2\sqrt{2}$ comes from a sine-modulated THz signal, which is detected as rms by the lock-in amplifier. Hence, the calculated responsivity represents the optical responsivity of the GFET detector with a bowtie antenna and a silicon lens. The noise source of a GFET THz detector is thermal Johnson-Nyquist noise, so NEP can be calculated as follows:

$$\text{NEP} = \sqrt{4k_B T R / R_V} \quad (2)$$

where k_B is the Boltzmann constant, T is the temperature, and $R = R_V/R_I$ is the drain-source resistance extracted from the voltage and current responsivities.

The voltage responsivity R_V and NEP versus gate voltage are shown in Fig. 5, which is the sample with the $n_0 = 4.5 \times 10^{15} \text{ m}^{-2}$. It shows a maximum responsivity of 74 V/W, with a minimum NEP of 130 $\text{pW}/\text{Hz}^{1/2}$. The maximum responsivity $R_{V \text{ MAX}}$ for other tested samples, is shown in Fig. 6 versus $1/n_0$.

V. DISCUSSION

For the configuration shown in Fig. 1, several models predict that the responsivity is proportional to the change in channel conductivity versus the gate voltage as [9], [18]:

$$\Delta U \propto \frac{1}{\sigma} \frac{\partial \sigma}{\partial V_g} \quad (3)$$

TABLE I
COMPARISON OF DETECTOR PERFORMANCES IN DIFFERENT TECHNOLOGIES

Technology	R_V , V/W	NEP, pW/Hz ^{1/2}	Frequency, GHz	Ref.
GFET	74	130 (<i>calculated</i>)	400	<i>This work</i>
GFET	14	515 (<i>calculated</i>)	600	[8]
Bilayer GFET	1.2	2000 (<i>calculated</i>)	370	[10]
MOSFET	5000	10 (<i>calculated</i>)	300	[2]
GaN HEMT	500	27 (<i>calculated</i>)	900	[6]
InP HEMT	26	–	300	[7]
Schottky	500	5 (<i>calculated</i>)	400	[21]
Bolometers	15	450 (<i>measured</i>)	330	[22]
Tunnel diodes	1150	0.4 (<i>measured</i>)	200	[23]

where ΔU is a rectified dc voltage, σ is a channel conductivity, and V_g is a difference between gate voltage and Dirac voltage. As a first order approximation, it qualitatively describes the measured data as shown in Fig. 5. The vertical shift is noticed between measured data and modeled curve. It can be associated with additional detection and mixing mechanisms that must be studied in more detail and which are outside the scope of this letter.

To find the maximum of the rectified dc voltage (3), one can use the derivative of $\partial\Delta U/\partial V_g$, using the following relation for σ [19]:

$$\sigma = q\mu n = q\mu\sqrt{n_0^2 + (V_g C_g/q)^2} \quad (4)$$

where q is electron charge, μ is mobility, and C_g is the gate capacitance per unit area which, in general, includes the gate dielectric, and quantum and interface capacitances [20]. Because of this, the maximum of ΔU at $\partial\Delta U/\partial V_g = 0$ reads as follows:

$$\Delta U_{\max} \propto \frac{C_g}{2n_0 q}. \quad (5)$$

As a first-order approximation, it shows that the maximum read-out voltage, or responsivity, is inversely proportional to n_0 .

The maximum measured responsivity versus $1/n_0$ is plotted in Fig. 6 for several samples, with n_0 varying from 4.5 to $8.4 \times 10^{15} \text{ m}^{-2}$. This includes results from [8], where $n_0 = 9.6 \times 10^{15} \text{ m}^{-2}$. The data is fitted with a $1/n_0$ function and shows a linear correlation in accordance with (5). The error bars take into account the uncertainty in the estimation of n_0 from [17] and uncertainty in power calibration and voltage readout during measurements.

With a previous best of 515 pW/Hz^{1/2} [8], the presented NEP and responsivity are, to our knowledge, the record low and record high, respectively, for graphene-based detectors. We attribute this to higher responsivity because of a reduced n_0 . For comparison, the responsivities and NEPs of the detectors in different technologies are compiled in Table I. For the GFET detectors, the values are worse than the best values achieved in, for example, MOSFET, GaN, or heterostructure backward tunnel diode detectors. The presented improvement indicates, though, that GFET detectors have the potential to increase their responsivity and reduce their NEP further to compete with other technologies.

VI. CONCLUSION

The highest reported responsivity of a GFET THz detector of 74 V/W was achieved and compared to the previous record of 14 V/W [8]. The calculated NEP is 130 pW/Hz^{1/2} at 400 GHz. It is shown that the responsivity is strongly influenced by the graphene/interface quality and degraded with the increase of

the residual carrier concentration n_0 in the graphene layer. This provides guidelines to develop more sensitive and competitive GFET detectors.

ACKNOWLEDGMENT

The authors would like to thank Dr. S. Cherednichenko for fruitful discussions and his support with measurements.

REFERENCES

- [1] S. Boppel *et al.*, "CMOS integrated antenna-coupled field-effect transistors for the detection of radiation from 0.2 to 4.3 THz," *IEEE Trans. Microw. Theory Techn.*, vol. 60, no. 12, pp. 3834–3843, Dec. 2012.
- [2] F. Schuster *et al.*, "Broadband terahertz imaging with highly sensitive silicon CMOS detectors," *Opt. Exp.*, vol. 19, no. 8, 2011, Art. no. 142605.
- [3] E. Öjefors, U. R. Pfeiffer, A. Lisauskas, and H. G. Roskos, "A 0.65 THz focal-plane array in a quarter-micron CMOS process technology," *IEEE J. Solid-State Circuits*, vol. 44, no. 7, pp. 1968–1976, Jul. 2009.
- [4] R. Al Hadi *et al.*, "A 1 k-pixel video camera for 0.7–1.1 terahertz imaging applications in 65-nm CMOS," *IEEE J. Solid-State Circuits*, vol. 47, no. 12, pp. 2999–3012, Dec. 2012.
- [5] S. Boppel *et al.*, "0.25- μm GaN TeraFETs optimized as THz power detectors and intensity-gradient sensors," *IEEE Trans. THz Sci. Technol.*, vol. 6, no. 2, pp. 348–350, Mar. 2016.
- [6] M. Bauer *et al.*, "High-sensitivity wideband THz detectors based on GaN HEMTs with integrated bow-tie antennas," in *Proc. 10th Eur. Conf. Microw. Integr. Circuits*, Paris, France, Sep. 2015, pp. 1–4.
- [7] T. Watanabe *et al.*, "InP- and GaAs-based plasmonic high-electron-mobility transistors for room-temperature ultrahigh-sensitive terahertz sensing and imaging," *IEEE Sensors J.*, vol. 13, no. 1, pp. 89–99, Jan. 2013.
- [8] A. Zak *et al.*, "Antenna-integrated 0.6 THz FET direct detectors based on CVD graphene," *Nano Lett.*, vol. 14, no. 10, pp. 5834–5838, 2014.
- [9] L. Vicarelli *et al.*, "Graphene field-effect transistors as room-temperature terahertz detectors," *Nat. Mater.*, vol. 11, pp. 865–871, 2012.
- [10] D. Spirito *et al.*, "High performance bilayer-graphene terahertz detectors," *Appl. Phys. Lett.*, vol. 104, 2014, Art. no. 061111.
- [11] A. Rogalski and F. Sizov, "Terahertz detectors and focal plane arrays," *Opto-Electron. Rev.*, vol. 19, no. 3, pp. 346–404, 2011.
- [12] A. Hsu *et al.*, "Impact of graphene interface quality on contact resistance and RF device performance," *IEEE Electron Device Lett.*, vol. 32, no. 8, pp. 1008–1010, Aug. 2011.
- [13] W. Bao *et al.*, "Lithography-free fabrication of high quality substrate-supported and freestanding graphene devices," *Nano Res.*, vol. 3, no. 2, pp. 98–102, 2010.
- [14] S. Adam, E. H. Hwang, V. M. Galitski, and S. Das Sarma, "A self-consistent theory for graphene transport," *Proc. Nat. Acad. Sci. USA*, vol. 104, no. 47, pp. 18392–18397, 2007.
- [15] J. Chan *et al.*, "Reducing extrinsic performance-limiting factors in graphene grown by chemical vapor deposition," *ASC Nano*, vol. 6, no. 4, pp. 3224–3229, 2012.
- [16] Graphenea Inc., [Online]. Available: <http://www.graphenea.com/>
- [17] O. Habibpour, J. Vukusic, and J. Stake, "A large-signal graphene FET model," *IEEE Trans. Electron Devices*, vol. 59, no. 4, pp. 968–975, Apr. 2012.
- [18] M. A. Andersson and J. Stake, "An accurate empirical model based on volterra series for FET power detectors," *IEEE Trans. Microw. Theory Techn.*, vol. 64, no. 5, pp. 1431–1441, May 2016.
- [19] V. E. Dorgan, M.-H. Bae, and E. Pop, "Mobility and saturation velocity in graphene on SiO₂," *Appl. Phys. Lett.*, vol. 97, 2010, Art. no. 082112.
- [20] M. Bonmann, A. Vorobiev, J. Stake, and O. Engström, "Effect of oxide traps on channel transport characteristics in graphene field effect transistors," *J. Vac. Sci. Technol. B, Microelectron. Process. Phenom.*, vol. 35, 2017, Art. no. 01A115.
- [21] L. Liu *et al.*, "A broadband quasi-optical terahertz detector utilizing a zero bias schottky diode," *IEEE Microw. Compon. Lett.*, vol. 20, no. 9, pp. 504–506, Sep. 2010.
- [22] S. Cherednichenko, A. Hammar, S. Bevilacqua, V. Drakinskiy, J. Stake, and A. Kalabukhov, "A room temperature bolometer for terahertz coherent and incoherent detection," *IEEE Trans. THz Sci. Technol.*, vol. 1, no. 2, pp. 395–402, Nov. 2011.
- [23] L. Liu *et al.*, "Advanced terahertz sensing and imaging systems based on integrated III-V interband tunneling devices," *Proc. IEEE*, vol. 105, no. 6, pp. 1020–1034, Jun. 2017.